Insights into Storm Direction Effect on Flood Response

Ganesh R. Ghimire[a,*], Navid Jadidoleslam[b], Radoslaw Goska[c], and Witold F. Krajewski[c]

[a] Environmental Sciences Division, Oak Ridge National Laboratory, Oak Ridge, Tennessee, U.S.

[b] School of Civil and Environmental Engineering, Georgia Institute of Technology, Atlanta, Georgia, U.S.

[c] Iowa Flood Center and IIHR-Hydroscience & Engineering, The University of Iowa, Iowa City, Iowa, U.S.

Submitted to *Journal of Hydrology*

October 2020

*Corresponding Author: Ganesh R. Ghimire (ghimiregr@ornl.gov)

Keywords: Basin Rotation Method, Synthetic Basin, Directional Effect, Flood Prediction, Hillslope-Link Model

Abstract

In this study, we investigate the directional influence of storm movement on catchment flood peak response using the synthetic circular basin. Due to the complexity in defining storm movements that require meteorological modeling, we adopt a novel approach of combining the basin rotation method (BRM) with a circular basin construct. A systematic basin rotation approach provides a proxy for the storm direction relative to the river network topology to study its hydrologic response. Using Stage-IV rainfall with 4-km by 1-hour resolution for 16 years period from 2003 to 2018 in Iowa, U.S., we systematically analyze consequent flood peak response due to storm directions (basin rotations) using a distributed hydrologic model called the Hillslope-Link Model (HLM). HLM has demonstrated the ability to reproduce observed streamflow for real river basins studied in Iowa. The hydrologic simulation results show that the BRM can quantify the relationship between the rainstorm direction and catchment hydrologic response. Also, the maximum flood peak response is strongly dependent on the interaction of the peak of the rainstorm with the peak of the width function. The results indicate significant differences in runoff volume and runoff peak and their interannual variability due to rainstorm direction. The study has important implications for flood frequency predictions and developing flood resilience and watershed management strategies, particularly due to changing storm tracks under a warming climate.

1. Introduction

The change in storm dynamics due to climate change is one of the most studied topics in recent years. Comprehensive climate models such as Global Circulation Models (GCM) along with observational data have indicated a poleward shift of storm tracks under a warming climate (e.g., Bengtsson et al., 2006; Mbengue and Schneider, 2013; Tamarin-Brodsky and Kaspi, 2017). Such a change in storm tracks has implications for pronounced changes in the regional climate and hydrological cycle. Therefore, understanding the interaction between the storm movement and the catchment hydrologic response provides important insights on flood risk and water resources management. It has been understood for a long time that storm movement has an impact on the shapes of hydrographs and peak hydrologic response. Numerous previous studies (e.g., De Lima et al., 2003; Foroud et al., 1984; Lee et al., 2015; Mizumura and Ito, 2011; Wu and Kurihara, 1996) have shown the impact of storm movement characteristics such as storm direction, intensity, and velocity on catchment hydrologic consequence. Here we provide insights into consequent streamflow response, particularly for both historical and potential future storm directions in a new framework.

To evaluate the impact of storm movement on hydrologic response, several approaches have been used. The most commonly used approaches are analytical (e.g., Jensen, 1984; Marcus, 1968; Singh, 2002, 1997), numerical (e.g., De Lima et al., 2003; Foroud et al., 1984; Liang, 2010; Nicótina et al., 2008; Niemczynowicz, 1991; Nunes et al., 2006; Surkan, 1974), and experimental (e.g., Black, 1972; De Lima et al., 2003; Marcus, 1968; Yen and Chow, 1969). These studies acknowledge that there is often a preferred storm direction for basins. For example, Foroud et al. (1984) studied the effect of rainstorm movement on flood runoff characteristics using a hypothetical rainstorm of 50 years return period, 75 mm depth, and 4

hours duration on a natural (real) watershed. Niemczynowicz (1984) investigated the relationship among storm movement characteristics such as storm duration, intensity, velocity, and direction and its impact on the catchment peak discharge. He referred to this impact as a directional bias. Using a conceptual catchment with meticulously designed geometry, he showed that the bias can even reach several hundred percent. Further, Ogden et al. (1995) explored the impact of rainfall movement on streamflow response in terms of the dimensionless hydrologic similarity parameters. Their results on a one-dimensional runoff plane show that the resulting peak flow effect is the maximum when the storm moves in the downslope direction with a dimensionless speed of 0.5. Also, they show that the conclusion holds for a complex natural topography. Liang (2010) and Volpi et al. (2013) investigated the rainstorm conditions in terms of direction, size, and velocity that lead to the enhancement of peak flow. Magnification of the peak flow also referred to as the resonance condition, occurs when the storm of size smaller than the basin moves along the main channel with the same speed as the flood wave (e.g., Ngirane-Katashaya and Wheater, 1985; Volpi et al., 2013). Volpi et al. (2013) in particular, illustrated that storm sizes much smaller than the dimension of the catchment result in a complete resonance effect irrespective of the combinations of the direction and speed of the moving rainstorm. Seo (2012) and Seo et al. (2012) explored the effect of storm movement on the runoff response of urban drainage networks considering cases of hypothetical rainstorms moving in upstream and downstream directions with varying speeds. Seo and Schmidt (2013) followed this study by investigating the relationship between channel sensitivity of hydrograph to rainstorm kinematics, including storm speeds, directions, and sizes adopting a circular synthetic catchment. These studies essentially demonstrate that the storm size smaller than the basin size traversing

down the main channel with the velocity equal to the average channel flow velocity results in the largest increase in the peak flow.

Many previous studies have used either synthetic catchment and/or rainstorms. Hence, generalizing our understanding of catchment hydrologic response from a single catchment or a rainstorm system is difficult. The notion behind using synthetic basins arises from the difficulty to manipulate the direction and speed of a real storm event (De Lima et al., 2003). Wright et al. (2014, 2013), for instance, advanced the methodology of stochastic storm transposition (SST) to produce realistic synthetic storms using temporal resampling and spatial transposition of selected storms derived from gridded datasets corresponding to the domain of interest. They used it to overcome the limited records of radar-based rainstorms in statistical studies of flood frequency. An alternative novel and simple to implement approach, the basin rotation method (BRM), was proposed by Lee et al. (2015) to investigate the directional influence of rainstorms on hydrologic response through its application to historical storm events on real drainage networks. Perez et al. (2019) used a similar approach to investigate a physics-based approach to flood frequency estimation. Most recently, Perez et al. (2021) have used both SST and BRM in their studies of flood frequency. However, Ghimire et al. (2021) among others, highlighted that basin rainfall volume bias is the single most important rainfall characteristic affecting catchment hydrologic response. Therefore, to isolate the storm directional effect and to generalize our understanding of the relationship between the rainstorm direction and catchment hydrologic response, particularly flood peak, an approach that allows rainfall volume conservation is needed. In this paper, we present such a framework that is novel, yet simple to implement even in real-world basins and discuss insight gained from its application.

We investigate two key questions: (1) Can BRM describe the relationship between rainstorm direction and catchment runoff (flood) response? (2) How does rainfall difference due to the directional influence of rainstorm propagate to the streamflow (peak) response? We answer these questions by organizing the paper as follows. In Section 2, we discuss the data used for this study. Section 3 describes the methods used to address our research question. In Section 4, we present key results from our analysis and the relevant discussion. Finally, Section 5 summarizes and lists some conclusions and limitations of this work.

2. Data

2.1 Synthetic catchment generation

When the same storm is passed over the same basin but rotated with respect to some arbitrary center of rotation, the storm volume affecting the basin changes, and thus the response differs. Therefore, it is difficult to distinguish the effect of the rotation from that of the changed volume. However, if the basin is circular and rotated about its center, there is no change in the volume under rotation. While there are no perfectly circular basins in nature, we can generate one synthetically to gain insights into the effect of the rotation.

We constructed a synthetic circular basin using the landscape evolution model developed by Campforts et al. (2017) and implemented it in TopoToolbox (Schwanghart and Scherler, 2014). The scheme is called TopoToolbox Landscape Evolution Model (TTLEM). Here we placed the basin (i.e., its center) at the center of the Cedar River basin near Cedar Rapids, Iowa (Fig. 1). The circular basin area is about 22,000 km^2, i.e. comparable to the Cedar River basin (20,800 km^2). TTLEM solves stream power river incision model using a flux-limiting finite volume method. TTLEM can account for three geological processes: tectonic deformations, river

131 incision, and hillslope processes. For our study, we adopted TTLEM parameter ranges provided
132 by Campforts et al. (2017) and followed their methodology. Table 1 provides a summary of the
133 TTLEM parameters used in our study. For more details on the processes, their numerical
134 solutions, and parameter ranges, readers are referred to Campforts et al. (2017).

135 We generated a circular Digital Elevation Model (DEM) with 80 km radius. The spatial
136 resolution of the DEM is approximately 70 m. The initial DEM for generating the circular basin
137 is a surface with a linear gradient towards the outlet of the basin with an elevation difference of
138 180 m between the highest elevation and the outlet elevation. The minimum elevation of the
139 initial surface is given as 1000 m to allow the evolution of processes. We perturbed the initial
140 elevations by additive noise drawn from a normal distribution with a zero mean and standard
141 deviation of 50 m. For tectonic deformation, we used a spatially uniform vertical uplift rate (U)
142 of 10^{-7} m/yr. We selected an implicit finite difference method to solve the river incision process
143 in TTLEM using a spatially uniform erodibility parameter (K) of 3×10^{-7}. For hillslope processes,
144 we used an implicit linear scheme with a threshold drainage area of 0.5 km^2, diffusivity
145 parameter (D) of 0.03 m^2/year, and threshold slope (S_c) of 0.5 m/m. We evolved the perturbed
146 DEM for 20 million years and subtracted the evolved surface elevation with the outlet's final
147 elevation to have an elevation range from 0 to 300 m. The result is the synthetic DEM shown in
148 Fig. 2a. We used this synthetic circular DEM to extract the river network and hillslopes. A
149 drainage area threshold of 0.5 km^2 was used for generating the stream network.

150 *2.2 River network topology and width function (WF)*

151 The consequent drainage network (stream order > 5) from a synthetic circular basin shown
152 in Fig. 2b looks almost symmetrical about the basin outlet with similar hillslope areas. The
153 system of hillslopes and streams (links) thus derived is an integral component of the Hillslope-

Link Model (HLM) modeling framework which we discuss later. The average hillslope area of the basin is about 0.65 km^2. There is a strong connection of flow aggregation, transport and hence hydrologic response with the spatial distribution of a drainage network characterized by its width function (e.g., Ghimire et al., 2020; Lee and Delleur, 1976; Perez et al., 2018a; Rodriguez-Iturbe and Rinaldo, 1997). The width function (WF) is the distribution of the number of links at a flow distance x from the outlet of the basin. In a discrete case, WF is given by (e.g., Perez et al., 2018a),

$$W(x) = \sum_{i=1}^{n} I_i(\mathrm{x}) \quad (1)$$

where $I(x)$ is an index function. $I(x)$ is defined as

$$I_i(x) = \begin{cases} 1, & x - \Delta x < D_i < x \\ 0, & otherwise \end{cases} \quad (2)$$

where D_i is the distance of the i^{th} link to the outlet of the basin, x is the distance to evaluate WF and Δx is the discretization interval of x. If the water in the drainage network travels to the outlet with the same (constant) velocity and the flow is not attenuated (e.g., Moussa, 2008), the width function can be interpreted as the distribution of travel times. We illustrate the drainage network in terms of D_i in Fig. 2b. The consequent WF illustrated in Fig. 2c shows a peak of $W(x)$ at about 275 km with a base of about 350 km. In hydrologic terms, the travel time of this synthetic circular basin is about 6 days assuming a constant channel velocity of 0.7 m/s.

One could test if the river network topology of a synthetic circular basin depicts some properties of natural stream networks. Also, the demonstration of our concept does not necessarily require real river networks. Here we test Horton laws for stream numbers, mean stream length, and mean basin area (refer to e.g., Scheidegger, 1968; Kirchner, 1993; Maritan et al., 1996 for details). The Horton ratios for stream numbers (R_B), mean stream length (R_L), and

mean basin area (R_A) for a circular basin are 1.99, 1.01, and 3.94, respectively (see Fig S1, supplementary information). The typical values of Horton ratios observed for natural stream networks are $3 \leq R_B \leq 5$, $1.5 \leq R_L \leq 3$, $3 \leq R_A \leq 6$ (Kirchner, 1993). The values of R_B and R_L for the synthetic basin are in the lower bound of the limit. Further, the Horton plots for each ratio show strong linear dependence in a log-linear space (Fig. S1) depicting Hortonian "laws" (Kirchner, 1993) reported for natural river networks. Perhaps the most important is the behavior of the area ratio as this is what controls the water volume from smaller to larger areas. Thus, a synthetic circular basin considered here suffices to explore the goals of this study, i.e. dependence of basin response on storm direction.

2.3 Basin rotation method (BRM)

A rainstorm can pass through a basin in several pathways. For most basins, however, there could be preferential (most frequent) pathways of rainstorms based on weather patterns, regional topography, and season. For instance, the most preferential pathway for the rainstorm in Iowa is the West-East (e.g., Perez et al., 2021). Fig. 3 demonstrates one such example. The catchment hydrologic response can vary depending on how rainstorm direction interacts with the basin WF. Such investigation requires meteorological simulation at high computation cost. Also, finding the center of the storm is a difficult task for such simulations. Hence, BRM (Lee et al., 2015) can be a much easier alternative to such an investigation, in which a catchment is rotated instead of a rainstorm. For example, rotating the basin in Fig. 2 at 90º in a counterclockwise direction is similar to the rainstorm passing through this basin from the North to South direction. In other words, it is the case of a rainstorm traversing downstream the basin. Further, BRM can provide insight on distinguishing the effect of radar or climate on the basin hydrologic response (peak). In this study, we rotate the basin about its center at every 15º in a counterclockwise direction

199 from 0º to 360º i.e. we have 24 different rainstorm pathways interacting with the drainage
200 network.

201 *2.4 Rainfall data*

202 For our analysis, we used 4-km hourly resolution Stage-IV rainfall data for Iowa as this is
203 the longest available radar-rainfall record. Stage-IV is the mosaicked national product at
204 National Center for Environmental Prediction (NCEP) from the regional hourly multi-sensor
205 (radar and gauges) precipitation analyses (MPEs) produced by the 12 River Forecast Centers
206 (RFC) over CONUS (NCEP, 2020). We employed Stage-IV rainfall data for years 2003-2018
207 for our investigation i.e. our analysis encompasses results from 16 years of hydrologic
208 simulations. The rainfall forcing (i.e., Stage-IV rainfall) to HLM using the circular basin scheme
209 is illustrated in Fig. 1.

210 *2.5 Hydrologic model*

211 To investigate the relationship between rainstorm movement (directional influence) and
212 runoff characteristics, we performed hydrologic simulations using HLM. HLM is the non-linear
213 physics-based distributed rainfall-runoff model, used by the Iowa Flood Center (IFC) for real-
214 time state-wide streamflow forecasting (e.g., Krajewski et al., 2017; Quintero et al., 2020, 2016).
215 This streamflow (flood) forecasting model conceptualizes landscape decomposition into a system
216 of hillslopes (areas) and links (stream segments) and has its roots in the scaling properties of
217 river networks (e.g., Ghimire et al., 2020; Gupta et al., 2015, 2010; Mantilla and Gupta, 2005).
218 Accordingly, the rainfall-runoff conversion process takes place at hillslopes and hence generated
219 flows route through corresponding links. HLM comprises four storage components to model
220 each hillslope-link system: channel storage $q(t)$ (m^3/s), pondage on the surface $S_p(t)$ (m), soil top

221 layer storage S_t *(t)* (*m*), and subsurface storage S_s*(t)* (*m*). Mathematically, it represents a system
222 of non-linear ordinary differential equations, which is solved using a numerical solver (Small et
223 al., 2013). HLM uses a non-linear velocity formulation for water transport and aggregates water
224 from upstream links. HLM, with its origin in the scaling properties of the river network, enables
225 us to perform scale-based analyses. Apart from being relatively simple to implement and not
226 calibrated in a traditional sense to any scale or rainfall product, HLM has shown skill in
227 reproducing observed runoff hydrographs across scales (e.g. Quintero et al. 2020). The
228 operational HLM uses a set of global parameters that work well on average across Iowa.
229 Because we collocate the circular basin at the center of the Cedar River basin in Iowa as a
230 testbed, using the same set of parameters across basin rotations (i.e., for storm directions) is a
231 reasonable choice. Refer to Krajewski et al. (2017), Quintero et al. (2016, 2020), and Ghimire et
232 al. (2020), among others for more details on the non-linear model structure of HLM.

233 ## 3. Methods

234 To make sure that we capture the effect of direction, we study the basin response for 24
235 angles of basin rotations, and for each, we used the same Stage-IV data as a rainfall input. For
236 the sake of brevity, we demonstrate in Fig. 3 the interaction of rainstorm with river network of
237 circular basin for every 45º rotation angle in the counterclockwise direction. The rainfall shown
238 here corresponds to the accumulation over September 2016. We use the rotation angle 0º,
239 defined here as the outlet of the basin pointing South, as the reference direction for the
240 evaluation of catchment streamflow response. This corresponds to the preferential West-East
241 storm direction in Iowa. As alluded to before, basin rotation of 90º is equivalent to the rainstorm
242 moving in the North-South direction. We provide these aspects for context only as in the study
243 we investigate directions on the full circle. The illustrations in Fig. 3 depict the interaction of

244 rainstorms with the WF of the drainage network rotated every 45º. They illustrate how
245 streamflow aggregation occurs through the river network and propagates to the basin outlet due
246 to the directional influence of rainstorms. For example, one can guess with reasonable certainty
247 that the largest and delayed streamflow peak response might occur at the basin outlet for the
248 reference direction. We derive this insight from the fact that if the peak of the rainstorm (red
249 color pixels) interacts with the peak of the WF that might result in the maximum peak flow
250 scenario. We present a detailed discussion of results from more extensive simulations in the next
251 section.

252 For our main analysis, we forced HLM with Stage-IV rainfall on annual basis from 2003 to
253 2018, for each of 24 angles. In total, we perform 384 hydrologic simulations. Further, the
254 analysis of 16 years of simulation allows us to distinguish the implications for streamflow
255 response between radar (e.g., algorithm changes, calibration strategies) and climate. We
256 performed hydrologic simulations for warm months i.e. from April 1 to December 1 for each
257 year. It is to avoid issues of snowstorms and snowmelt; HLM shows the best performance
258 during these months. For each year, we kept the initial conditions (for April 1) of hydrologic
259 simulations the same across all 24 basin rotations i.e., the storm directions. We investigated both
260 the streamflow (peak) response at the basin outlet for each direction of the rainstorm and the
261 behavior of runoff response relative to that of the reference direction. This reference allows us to
262 quantify the directional effect of rainstorms. We will generalize it more in the next section. We
263 quantified the relative rainfall difference in terms of rainfall volume difference (*RFVD*) and
264 runoff difference in terms of runoff volume difference (*RVD*), and peak difference (*PD*). Details
265 of their computation are presented in Appendix A. We evaluated these relationships across three
266 different time scales: annual scale, annual peak event scale, and multiple-events scale over the

267 threshold. The annual peak event corresponds to the rainfall-runoff associated with the annual
268 maximum flow. We adopted a threshold equivalent to a two-year return period flood at the
269 Cedar River basin outlet (~350 m^3/s) to qualify multiple peak events for each year of simulation.
270 The flow chart presented in Fig. 4 summarizes the entire procedure adopted in this study.

271 4. Results and Discussion

272 In this section, we present the key results from the application of BRM demonstrating the
273 relationship between rainstorm movement (directional influence) and streamflow (flood)
274 response. First, we show in Fig. 5 the simulation hydrographs at the basin outlet across different
275 basin orientations for a clear demonstration of understanding the streamflow (flood) response to
276 rainfall shown in Fig. 3. The hydrographs correspond to a major flood event in the period of
277 September 15 - October 15, 2016. The simulation hydrographs show that the maximum flood
278 peak occurs for the reference direction. The streamflow (peak) response is the result of the
279 interaction of rainstorm direction illustrated by angles of rotation with the drainage network or
280 the WF. Along the reference direction, the rainstorm peak (red color pixels in Fig. 3) moves
281 West-East through the peak of the WF interacting with a large number of hillslopes. Also, note
282 the delayed timing of this peak as the rainstorm center is most distant from the basin outlet. The
283 response is not that different for 315°. Also, note the unimodal and bimodal peaks across basin
284 rotations. For instance, rotation angles 45°, 90°, 135°, and 180° result in bimodal peaks. For
285 these directions, the rainstorm peaks (see Fig. 3) interact with the WF at a significant distance
286 from each other. The resulting runoff peak is the lowest for the 90º rotation angle i.e. when a
287 rainstorm is moving North-South. It is because the peak of a rainstorm (red color pixels in Fig.
288 3) interacts with a smaller number of streams, which are a shorter distance from the basin outlet
289 i.e. less than the distance to the peak of the WF. The peak of the rainstorm in Fig. 3 passes

through the hillslopes (streams) at the shortest distance from the basin outlet at the 135º rotation angle, hence the earliest peak (see Fig. 5). The timing of this peak is not that different for 180°. The difference in magnitude of the peak between the two emanates from the interaction of the peak of the rainstorm with a larger number of hillslopes despite their similar spatial distribution. The results presented here are in qualitative agreement with the findings from previous studies (e.g., Black, 1972; De Lima et al., 2003; Foroud et al., 1984; Lee et al., 2015).

In addition to the utility of BRM in investigating the relationship between the interaction of rainstorm movement with WF and streamflow response, it is of interest to the hydrologic community to gain insights on the propagation of rainfall difference to the streamflow response. Fig. 6 presents the percentile plots of relative differences in rainfall-runoff across 24 different basin orientations evaluated at an annual scale. The essence of the percentile plot is similar to the boxplot, showing the interannual variability over 16 years (2003-2018). Each color code depicts a range of percentiles. It represents the interannual variability conditional on the basin rotation angle (i.e., the storm direction). For instance, the range [75, 25] demonstrates the interquartile range (Fig. 6). The median and interquartile range of rainfall volume difference (*RFVD*) across basin rotations is close to 0 (see Fig. 6a). It suggests that, as expected, the rainfall volume is preserved in the basin rotation process. The small differences are due to the border effects (note that the Stage IV grid is not Cartesian; see the grid in Fig. 1). In Figs. 6b and 6c, we show the consequent runoff volume difference (*RVD*) and runoff peak difference (*PD*), respectively. Clearly, both metrics on runoff characteristics show a systematic pattern with storm directions. The median *RVD* (i.e., the solid dark line) does not depart significantly from the zero line while the largest interquartile range is about 10% at 105º (285º) rotation angle (see Fig. 6b). It is to suggest that the largest variability of *RVD* occurs when the rainstorm moves at

313 105º clockwise (285º) relative to the reference (i.e., most frequent storm direction in Iowa, West-
314 East).

315 Fig. 6c shows that the largest median *PD* is about 20% at 285º (median *PD* at 105º is ~15%)
316 while the largest interquartile range is about 45% at the rotation angle of 105º (285º). The results
317 show that the peak runoff shows the largest difference as well as interannual variability among
318 the three. Though it is difficult to distinguish the complex interaction of directional influence
319 with the non-linear structure of the hydrologic model, one can at least gain credible insight into
320 the pattern of flood peak response. Note that there are few outliers (not shown) in the runoff
321 characteristics beyond the 90-percentile range. For instance, the maximum *PD* as large as
322 ~150% results from the storm direction effect. Interestingly, these outliers correspond to the dry
323 years in Iowa in the study period, including 2003, 2006, and 2011. Fig. S2 (supplementary
324 information) demonstrates the directional effect for two such representative years: 2011
325 (relatively dry) and 2016 (relatively wet). For both years, the pattern is similar but a significant
326 difference in magnitude. The largest difference in 2011 i.e., for ~105° (285°) is the case of
327 smaller storm size traversing the basin. It is hard, however, to determine whether this resulted in
328 the resonance condition. Overall, despite negligible interannual variability of *RFVD* (Fig. 6a),
329 the significant increase in the median and variability in *RVD* and *PD* suggests the contribution
330 from the spatial variability of rainfall due to storm direction. We used a large ensemble of real
331 rainstorms with varying size, intensity, duration, and velocity over 16 years, which lead to the
332 interannual variability. Even for a single storm direction, these characteristics interact in
333 complex ways with the basin characteristics (such as storm velocity with the channel flow
334 velocity). Also, radar-rainfall uncertainty contributes to the interannual variability, particularly
335 for the drier period. As alluded to before, somewhat of the periodic behavior in Fig. 6 is due to

the interaction of rainstorms with different portions of the WF. In the process, when they affect a larger number of hillslopes despite being at a similar distance from the outlet, they result in larger peaks, hence the difference across basin rotations (i.e., storm directions). It is, however, difficult to distinguish whether any of these rainstorm conditions lead to a resonance condition for the synthetic basin.

Evaluating the interaction between storm direction and streamflow (flood) response requires one to investigate the dependence across timescales, which helps to generalize our results. Therefore, In Fig. 7 we present the results of a similar analysis as in Fig.6 but for the annual peak event. The median *RFVD* is close to 0 and the corresponding variability (i.e., interquartile range) is about 10% (Fig. 7a). The consequent median *RVD* is about 15% while the corresponding variability is about 20% for the rotation angle of 105º (Fig. 7b). Likewise, the resulting median *PD* is about 25% with the corresponding variability of about 40% when the storm moves at 105º clockwise relative to the reference direction (Fig. 7c). Likewise, Fig. 8 presents the results for multiple peak events above a threshold (~350 m^3/s). Clearly, this definition generates the largest sample of flood peak events across 16 years. The consequent runoff characteristics (both *RVD* and *PD*) follow a similar pattern in terms of median values as well as their interannual variability. The periodic pattern here is clear, which we can attribute to the definition of events over a threshold. The results from 16 years of the analysis presented in Figs. 6-8 show a similar relationship between rainfall characteristics i.e. *RFVD* and consequent runoff characteristics i.e. *RVD* and *PD*. The pattern of runoff response due to storm direction is similar to those reported previously, for example, the most recent work by Perez et al. (2021) using Iowa as a testbed. This experiment uses the synthetic basin commensurate with the scale of storm size to implement our framework. For such scenarios, we demonstrated that runoff response, particularly flow

peak is significantly affected by storm direction. One could also investigate the effect on basin scales in this framework. Studies (e.g., Ogden et al., 1995; Perez et al., 2021; Volpi et al., 2013) show that basins much smaller (or much larger) relative to the storm size result in a minimal directional effect. Thus, we argue that the scale of the synthetic basin adopted for this study suffices to demonstrate insights into directional effect using the framework.

5. Conclusions

In this paper, we investigated the relationship between the rainstorm direction and the catchment hydrologic response using a synthetic circular basin. We used a novel approach called BRM in which we rotated the basin instead of the storm. We used 16 years of Stage-IV rainfall data from 2003 to 2018 for Iowa. The rainfall was forced to HLM on an annual basis across 24 basin orientations between 0º and 360º at every 15º. Our hydrologic simulation experiment demonstrates that BRM can quantify the relationship between the rainstorm direction and the consequent hydrologic response. The method is simple to implement and obviates the need to perform a large number of meteorological simulations at a much-reduced computational cost.

Our results show that the peak flow response is strongly dependent on the interaction of the peak of the rainstorm with the peak of the WF. The runoff characteristics, including *RVD* and *PD* at all three-time scales of annual, event, and multi-event scales due to the directional effect of rainstorms show virtually a periodic pattern. The results show the largest median *PD* of up to 25% with a corresponding interquartile range of up to 40%. In other words, the directional effect on peak flow response is significant particularly for basin scales commensurate with the storm size. The results of this paper have important implications for streamflow (flood) predictions,

best management practices, and flood mitigation efforts. The results are pertinent as the scientific community recognizes that storm tracks may be changing under a warming climate. One should be cautious in understanding the value of these differences, particularly from the flood protection structures' design standpoint. For instance, the largest *PD* of ~50% in 2016 is more relevant than the largest PD of ~150% in 2011 (see Fig. S2) as the flood in 2016 is about 15 times as large. Nonetheless, the result is significant considering the difference can be attributed mostly to the directional effect of the rainstorm. Also, this approach can provide an easier framework for performing the hydrologic simulation-based experiment for flood frequency analysis, which typically does not account for the storm direction effect on peak flow distribution (e.g., Perez et al., 2021).

This study is not without some limitations. To be able to distinguish the error in runoff response from rainfall volume bias and directional effect, we adopted a construct of the synthetic circular basin. The total rainfall volume is preserved under rotation for the circular basin. Its use demonstrates the effect of storm direction on the response due to the interactions of the storm patterns with the width function of the basin. However, although the total rainfall volume is directionally invariant for the entire basin, this is not true for the numerous sub-basins. This implies that there is a limited benefit of the circular basin concept for studies of peak flow scaling (e.g., Ayalew et al., 2014; Mantilla, 2007; Menabde et al., 2001) and regional flood frequency analysis (e.g., Gupta and Dawdy, 1995; Perez et al., 2019a, 2019b, 2018a, 2018b). Moreover, we assume that the radar-rainfall characteristics, including retrieval algorithms, and quality control stayed the same over the 16 years of the analysis period. Therefore, using the BRM framework for a large ensemble of storms with varying speed, size, intensity, and spatial

403 footprint across a range of real-world basins could provide a more comprehensive insight into
404 storm-basin interaction studies in the future.

Appendix A

We compute relative differences of rainfall and runoff across angles of rotation of basins for our hydrologic simulations. Our reference hydrograph corresponds to the reference scenario of storm traversing in the most frequent direction of West-East in Iowa (rotation angle = 0º). The subscripts '*r*' and '*s*' refer to the reference and simulated (other rotation angles) variables, respectively. We compute rainfall volume difference (*RFVD*) as,

$$\boldsymbol{RFVD} = \frac{(\boldsymbol{rfv_s} - \boldsymbol{rfv_r})}{\boldsymbol{rfv_r}} \times \mathbf{100} \quad \text{(A.1)}$$

where *rfv* is the rainfall volume. Likewise, runoff volume difference (*RVD*) is given by,

$$\boldsymbol{RVD} = \frac{(\boldsymbol{rv_s} - \boldsymbol{rv_r})}{\boldsymbol{rv_r}} \times \mathbf{100} \quad \text{(A.2)}$$

where *rv* is the runoff volume. The peak difference (*PD*) is given by,

$$\boldsymbol{PD} = \frac{(\boldsymbol{peak_s} - \boldsymbol{peak_r})}{\boldsymbol{peak_r}} \times \mathbf{100} \quad \text{(A.3)}$$

where *peak* refers to the streamflow peak. We similarly compute these three metrics for three-time scales: annual scale, annual peak event scale, and multiple-events scales over a threshold.

Declarations of Competing Interest

The authors declare that they have no known competing financial interests or personal relationships that could have appeared to influence the work reported in this paper.

Acknowledgments and Data

The study was conducted when GRG and NJ were with the Iowa Flood Center. The authors acknowledge the IFC at the University of Iowa for providing financial support for this work. The last author acknowledges partial support of the Rose & Joseph Summers endowment. The

rainfall data supporting this study can be obtained from http://s-iihr51.iihr.uiowa.edu/precipitation/stage4/ . The results of this study can be found at https://github.com/ganeshghimire1986/basin_rotation_method.

References

Ayalew, T.B., Krajewski, W.F., Mantilla, R., 2014. Connecting the power-law scaling structure of peak-discharges to spatially variable rainfall and catchment physical properties. Adv. Water Resour. 71, 32–43. https://doi.org/10.1016/j.advwatres.2014.05.009

Bengtsson, L., Hodges, K.I., Roeckner, E., 2006. Storm tracks and climate change. J. Clim. 19, 3518–3543. https://doi.org/10.1175/JCLI3815.1

Black, P.E., 1972. Hydrograph responses to geomophic watershed characteristics and precipitation precipitation variables 17, 309–329.

Campforts, B., Schwanghart, W., Govers, G., 2017. Accurate simulation of transient landscape evolution by eliminating numerical diffusion: The TTLEM 1.0 model. Earth Surf. Dyn. 5, 47–66. https://doi.org/10.5194/esurf-5-47-2017

De Lima, J.L.M.P., Singh, V.P., De Lima, M.I.P., 2003. The influence of storm movement on water erosion: Storm direction and velocity effects. Catena 52, 39–56. https://doi.org/10.1016/S0341-8162(02)00149-2

Foroud, N., Broughton, R.S., Austin, G.., 1984. The effect of a moving rainstorm on a direct runoff properties. Am. Water Resour. Assoc. 20, 87–92.

Ghimire, G.R., Krajewski, W.F., Ayalew, T., Goska, R., 2021. Hydrologic investigations of radar-rainfall error propagation to hydrographs (in preparation). J. Hydrol.

Gupta, V.K., Ayalew, T.B., Mantilla, R., Krajewski, W.F., 2015. Classical and generalized horton laws for peak flows in rainfall-runoff events. Chaos 25. https://doi.org/10.1063/1.4922177

Gupta, V.K., Dawdy, D.R., 1995. Physical interpretations of regional variations in the scaling exponents of flood quantiles. Hydrol. Process. 9, 347–361. https://doi.org/10.1002/hyp.3360090309

Gupta, V.K., Mantilla, R., Troutman, B.M., Dawdy, D., Krajewski, W.F., 2010. Generalizing a nonlinear geophysical flood theory to medium-sized river networks. Geophys. Res. Lett. 37, 1–6. https://doi.org/10.1029/2009GL041540

Jensen, M., 1984. Runoff pattern and peak flows from moving block rains based on a linear time-area curve. Nord. Hydrol. 15, 155–168. https://doi.org/10.2166/nh.1984.0012

Kirchner, J.W., 1993. 1993_18_Hortons_laws.pdf.

458 Krajewski, W.F., Ceynar, D., Demir, I., Goska, R., Kruger, A., Langel, C., Mantilllla, R.,
459 Niemeier, J., Quintero, F., Seo, B.C., Smallll, S.J., Weber, L.J., Young, N.C., 2017. Real-
460 time flood forecasting and information system for the state of Iowa. Bull. Am. Meteorol.
461 Soc. 98, 539–554. https://doi.org/10.1175/BAMS-D-15-00243.1
462 Lee, M.T., Delleur, J.W., 1976. A variable source area model of the rainfall-runoff process based
463 on the Watershed Stream Network. Water Resour. Res. 12, 1029–1036.
464 https://doi.org/10.1029/WR012i005p01029
465 Lee, T., Shin, J., Park, T., Lee, D., 2015. Basin rotation method for analyzing the directional
466 influence of moving storms on basin response. Stoch. Environ. Res. Risk Assess. 29, 251–
467 263. https://doi.org/10.1007/s00477-014-0870-y
468 Liang, J., 2010. Evaluation of runoff response to moving rainstorms. System. University of
469 Wisconsin, Miluwakee.
470 Mantilla, R., 2007. Physical basis of statistical scaling in peak flows and stream flow
471 hydrographs for topologic and spatially embedded random self-similar channel networks.
472 ProQuest Diss. Publ. University of Colorado at Boulder.
473 Mantilla, R., Gupta, V.K., 2005. A GIS numerical framework to study the process basis of
474 scaling statistics in river networks. IEEE Geosci. Remote Sens. Lett. 2, 404–408.
475 https://doi.org/10.1109/LGRS.2005.853571
476 Marcus, N., 1968. A laboratory and analytical study of surface runoff under moving rainstorms.
477 University of Illinois at Urbana-Champaign.
478 Maritan, A., Rinaldo, A., Rigon, R., Giacometti, A., Rodríguez-Iturbe, I., 1996. Scaling laws for
479 river networks. Phys. Rev. E - Stat. Physics, Plasmas, Fluids, Relat. Interdiscip. Top. 53,
480 1510–1515. https://doi.org/10.1103/PhysRevE.53.1510
481 Mbengue, C., Schneider, T., 2013. Storm track shifts under climate change: What can be learned
482 from large-scale dry dynamics. J. Clim. 26, 9923–9930. https://doi.org/10.1175/JCLI-D-13-
483 00404.1
484 Menabde, M., Veitzer, S., Gupta, V., Sivapalan, M., 2001. Tests of peak flow scaling in
485 simulated self-similar river networks. Adv. Water Resour. 24, 991–999.
486 https://doi.org/10.1016/S0309-1708(01)00043-4
487 Mizumura, K., Ito, Y., 2011. Influence of moving rainstorms on overland flow of an open book
488 type using kinematic wave. J. Hydrol. Eng. 16, 926–934.

https://doi.org/10.1061/(ASCE)HE.1943-5584.0000398
Moussa, R., 2008. What controls the width function shape, and can it be used for channel network comparison and regionalization? Water Resour. Res. 44, 1–19. https://doi.org/10.1029/2007WR006118
NCEP, 2020. National Stage IV QPE Product [WWW Document].
Ngirane-Katashaya, G.G., Wheater, H.S., 1985. Hydrograph Sensitivity to Storm Kinematics. Water Resour. Res. 21, 337–345. https://doi.org/10.1029/WR021i003p00337
Nicótina, L., Alessi Celegon, E., Rinaldo, A., Marani, M., 2008. On the impact of rainfall patterns on the hydrologic response. Water Resour. Res. 44, 1–14. https://doi.org/10.1029/2007WR006654
Niemczynowicz, J., 1991. On storm movement and its applications. Atmos. Res. 27, 109–127. https://doi.org/10.1016/0169-8095(91)90012-L
Niemczynowicz, J., 1984. Investigation of the influence of rainfall movement on runoff hydrograph. Part I - simulation on conceptual catchment (Lund). Nord. Hydrol. 15, 57–70. https://doi.org/10.2166/nh.1984.0005
Nunes, J.P., de Lima, J.L.M.P., Singh, V.P., de Lima, M.I.P., Vieira, G.N., 2006. Numerical modeling of surface runoff and erosion due to moving rainstorms at the drainage basin scale. J. Hydrol. 330, 709–720. https://doi.org/10.1016/j.jhydrol.2006.04.037
Ogden, F.L., Richardson, J.R., Julien, P.Y., 1995. Similarity in catchment response: 2. Moving rainstorms. Water Resour. Res. 31, 1543–1547. https://doi.org/10.1029/95WR00519
Perez, G., Gomez-Velez, J.D., Mantilla, R., Wright, D.B., Li, Z., 2021. The Effect of Storm Direction on Flood Frequency Analysis. Geophys. Res. Lett. 48. https://doi.org/10.1029/2020GL091918
Perez, G., Mantilla, R., Krajewski, W.F., 2018a. The influence of spatial variability of width functions on regional peak flow regressions. Water Resour. Res. 54, 7651–7669. https://doi.org/10.1029/2018WR023509
Perez, G., Mantilla, R., Krajewski, W.F., 2018b. Advances in Nonlinear Geosciences. Adv. Nonlinear Geosci. 497–518. https://doi.org/10.1007/978-3-319-58895-7
Perez, G., Mantilla, R., Krajewski, W.F., Quintero, F., 2019a. Examining observed rainfall, soil moisture, and river network variabilities on peak flow scaling of rainfall-runoff events with implications on regionalization of peak flow quantiles. Water Resour. Res. 55, 10707–

10726. https://doi.org/10.1029/2019WR026028

Perez, G., Mantilla, R., Krajewski, W.F., Wright, D.B., 2019b. Using physically based synthetic peak flows to assess local and regional flood frequency analysis methods. Water Resour. Res. 55, 8384–8403. https://doi.org/10.1029/2019WR024827

Quintero, F., Krajewski, W.F., Mantilla, R., Small, S., Seo, B.C., 2016. A spatial-dynamical framework for evaluation of satellite rainfall products for flood prediction. J. Hydrometeorol. 17, 2137–2154. https://doi.org/10.1175/JHM-D-15-0195.1

Quintero, F., Krajewski, W.F., Seo, B.C., Mantilla, R., 2020. Improvement and evaluation of the Iowa Flood Center Hillslope Link Model (HLM) by calibration-free approach. J. Hydrol. 584, 124686. https://doi.org/10.1016/j.jhydrol.2020.124686

Rodriguez-Iturbe, I., Rinaldo, A., 1997. Fractal river basins: chance and self-organization, Cambridge University Press.

Scheidegger, A.E., 1968. Horton's laws of stream numbers and a temperature-analog in river nets. Water Resour. Res. 4, 167–171.

Schwanghart, W., Scherler, D., 2014. Short Communication: TopoToolbox 2 - MATLAB-based software for topographic analysis and modeling in Earth surface sciences. Earth Surf. Dyn. 2, 1–7. https://doi.org/10.5194/esurf-2-1-2014

Seo, Y., 2012. The effect of rainstorm movement on urban drainage network runoff hydrographs. University of Illinois at Urbana-Champaign.

Seo, Y., Schmidt, A.R., 2013. Network configuration and hydrograph sensitivity to storm kinematics. Water Resour. Res. 49, 1812–1827. https://doi.org/10.1002/wrcr.20115

Seo, Y., Schmidt, A.R., Sivapalan, M., 2012. Effect of storm movement on flood peaks: Analysis framework based on characteristic timescales. Water Resour. Res. 48, 1–12. https://doi.org/10.1029/2011WR011761

Singh, V.P., 2002. Effects of storm direction and duration on infiltrating planar flow with partial coverage. Hydrol. Process. 19, 969–992. https://doi.org/10.1002/hyp.5554

Singh, V.P., 1997. Effect of spatial and temporal variability in rainfall and watershed characteristics on stream flow hydrograph. Hydrol. Process. 11, 1649–1669. https://doi.org/10.1002/(SICI)1099-1085(19971015)11:12<1649::AID-HYP495>3.0.CO;2-1

Small, S.J., Jay, L.O., Mantilla, R., Curtu, R., Cunha, L.K., Fonley, M., Krajewski, W.F., 2013.

551 An asynchronous solver for systems of ODEs linked by a directed tree structure. Adv.
552 Water Resour. 53, 23–32. https://doi.org/10.1016/j.advwatres.2012.10.011
553 Surkan, A.J., 1974. Simulation of storm velocity effects on flow from distributed channel
554 networks. Water Resour. Res. 10, 1149–1160. https://doi.org/10.1029/WR010i006p01149
555 Tamarin-Brodsky, T., Kaspi, Y., 2017. Enhanced poleward propagation of storms under climate
556 change. Nat. Geosci. 10, 908–913. https://doi.org/10.1038/s41561-017-0001-8
557 Volpi, E., Di Lazzaro, M., Fiori, A., 2013. Analytical modeling of the hydrologic response under
558 moving rainstorms: Storm-catchment interaction and resonance. J. Hydrol. 493, 132–139.
559 https://doi.org/10.1016/j.jhydrol.2013.04.025
560 Wright, D.B., Smith, J.A., Baeck, M.L., 2014. Flood frequency analysis using radar rainfall
561 fields and stochastic storm transposition. Water Resour. Res. 50, 1592–1615.
562 https://doi.org/10.1002/2013WR014224
563 Wright, D.B., Smith, J.A., Villarini, G., Baeck, M.L., 2013. Estimating the frequency of extreme
564 rainfall using weather radar and stochastic storm transposition. J. Hydrol. 488, 150–165.
565 https://doi.org/10.1016/j.jhydrol.2013.03.003
566 Wu, C.C., Kurihara, Y., 1996. A numerical study of the feedback mechanisms of hurricane-
567 environment interaction on hurricane movement from the potential vorticity perspective. J.
568 Atmos. Sci. https://doi.org/10.1175/1520-0469(1996)053<2264:ANSOTF>2.0.CO;2
569 Yen, B.C., Chow, V. Te, 1969. A laboratory study of surface runoff due to moving rainstorms.
570 Water Resour. Res. 5, 989–1006. https://doi.org/10.1029/WR005i005p00989

List of Tables

Table 1: TopoToolbox Land Evolution Model (TTLEM) parameters used for generating the synthetic circular basin.

Parameter	Unit	Selected
Initialization		
Initial Surface	-	Linear gradient
Uplift Pattern	-	Uniform
Uplift rate	$m.yr^{-1}$	10^{-3}
Spatial Step	m	70
Boundary Conditions		
Boundary Condition Type	-	Dirichlet
Computational Parameters		
Timespan	yr	20×10^{6}
Outer time step	yr	1×10^{6}
Domain shape	-	Circle
Drainage area threshold	m^2	$5x10^{6}$
Drainage network	-	Variable
River Incision		
K	$m^{1-2m} .yr^{-1}$	$3x10^{-7}$
m		0.5
n		1
Hillslope Response		
D	$m^2. yr^{-1}$	0.03
Sc	$m.m^{-1}$	0.8
Numerical Schemes		
River incision	-	Implicit FDM
CFL	-	0.95
Hillslope Diffusion	-	Implicit linear with threshold slope

List of Figures

variability over the years 2003-2018 with every 5-percentile interval. For instance, [95,5] represents the range between 95^{th} and 5^{th} percentiles, [75,25] represents the range between 75^{th} and 5^{th} percentiles (i.e., interquartile range), and so on. (a) Rainfall volume difference (*RFVD*) (b) Runoff volume difference (*RVD*), and (c) Peak difference (*PD*).

Figure 7: Percentile plots showing the relationship of rainfall-runoff metrics with angles of basin rotation evaluated for the annual peak event. Each color code represents percentiles of interannual variability over the years 2003-2018 with every 5-percentile interval. For instance, [95,5] represents the range between 95^{th} and 5^{th} percentiles, [75,25] represents the range between 75^{th} and 5^{th} percentiles (i.e., interquartile range), and so on. (a) *RFVD* (b) *RVD*, and (c) *PD*.

Figure 8: Percentile plots showing the relationship of rainfall-runoff metrics with angles of basin rotation evaluated for multiple peaks over the threshold. Each color code represents percentiles of interannual variability over the years 2003-2018 with every 5-percentile interval. For instance, [95,5] represents the range between 95^{th} and 5^{th} percentiles, [75,25] represents the range between 75^{th} and 5^{th} percentiles (i.e., interquartile range), and so on. (a) *RFVD* (b) *RVD*, and (c) *PD*.

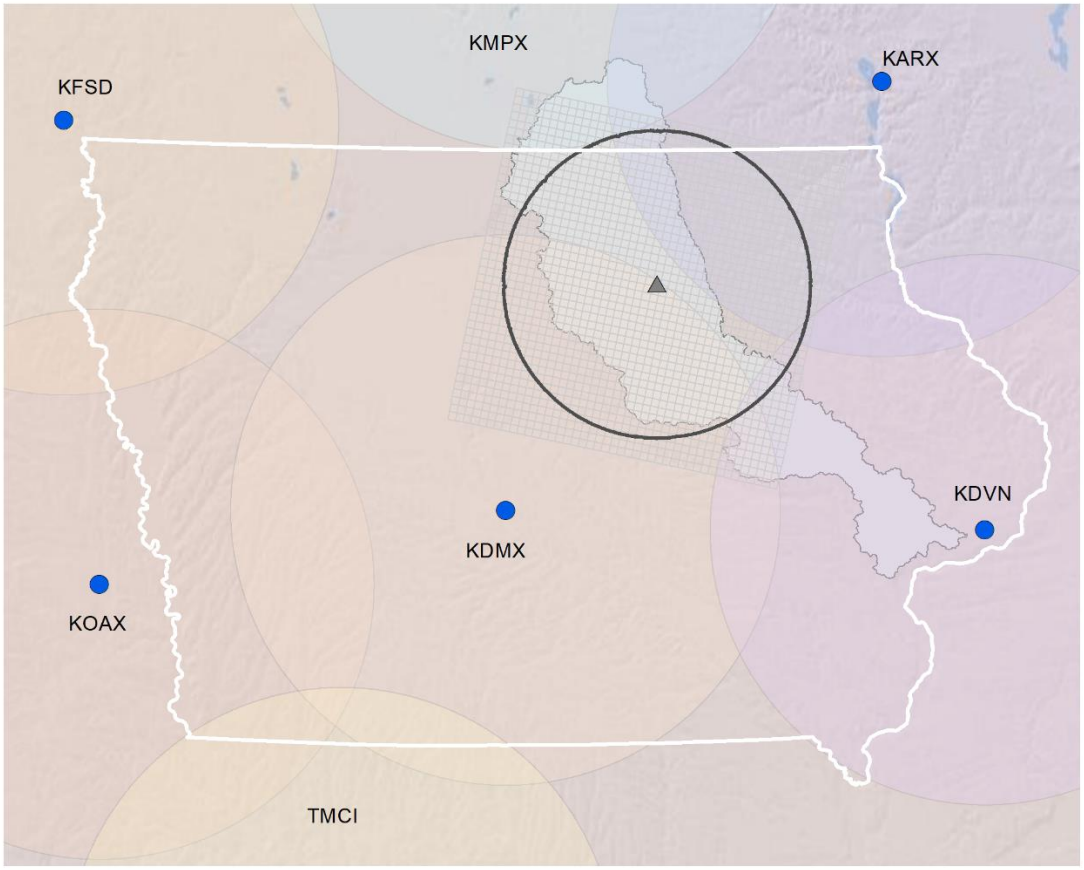

612

613 Figure 1: Demonstration of a synthetic circular basin, the centroid of which is collocated with the
614 centroid of the Cedar River basin. The solid white boundary represents the state of Iowa, which
615 is overlooked by seven NEXRAD radars for continuous rainfall observation. The circles around
616 these radars correspond to the range of 150 km. The underlying grid represents the Stage-IV
617 rainfall.

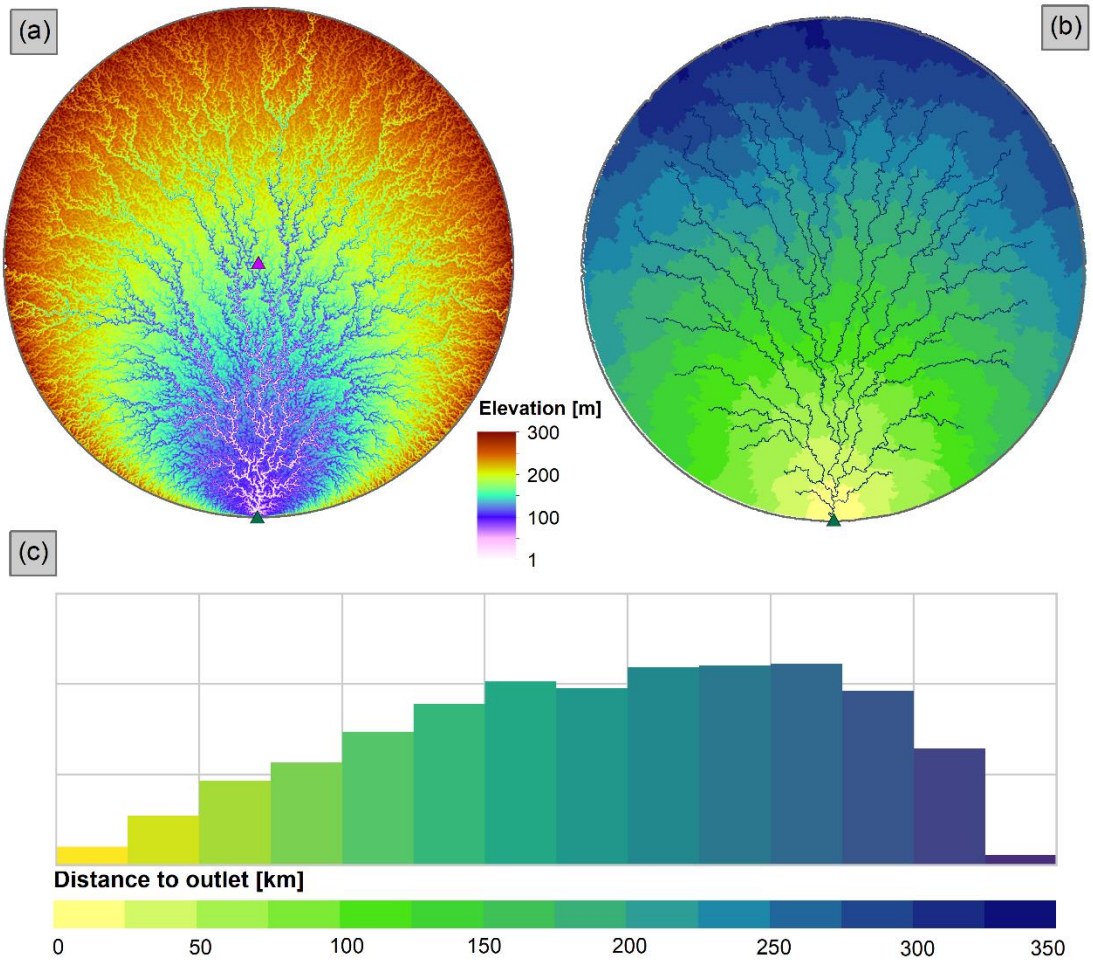

618

619 Figure 2: River network geometry of the synthetic circular basin. (a) Synthetic digital elevation
620 model (DEM) (b) Hillslopes overlain by river network corresponding to the DEM in (a). The
621 minimum stream order shown here is 5. The color code represents the distance in kilometers to
622 the basin outlet. (c) Width function (WF) of the river network in (b). The horizontal axis
623 corresponds to the distance to the outlet while the vertical axis corresponds to counts. The color
624 code complements that of (b).

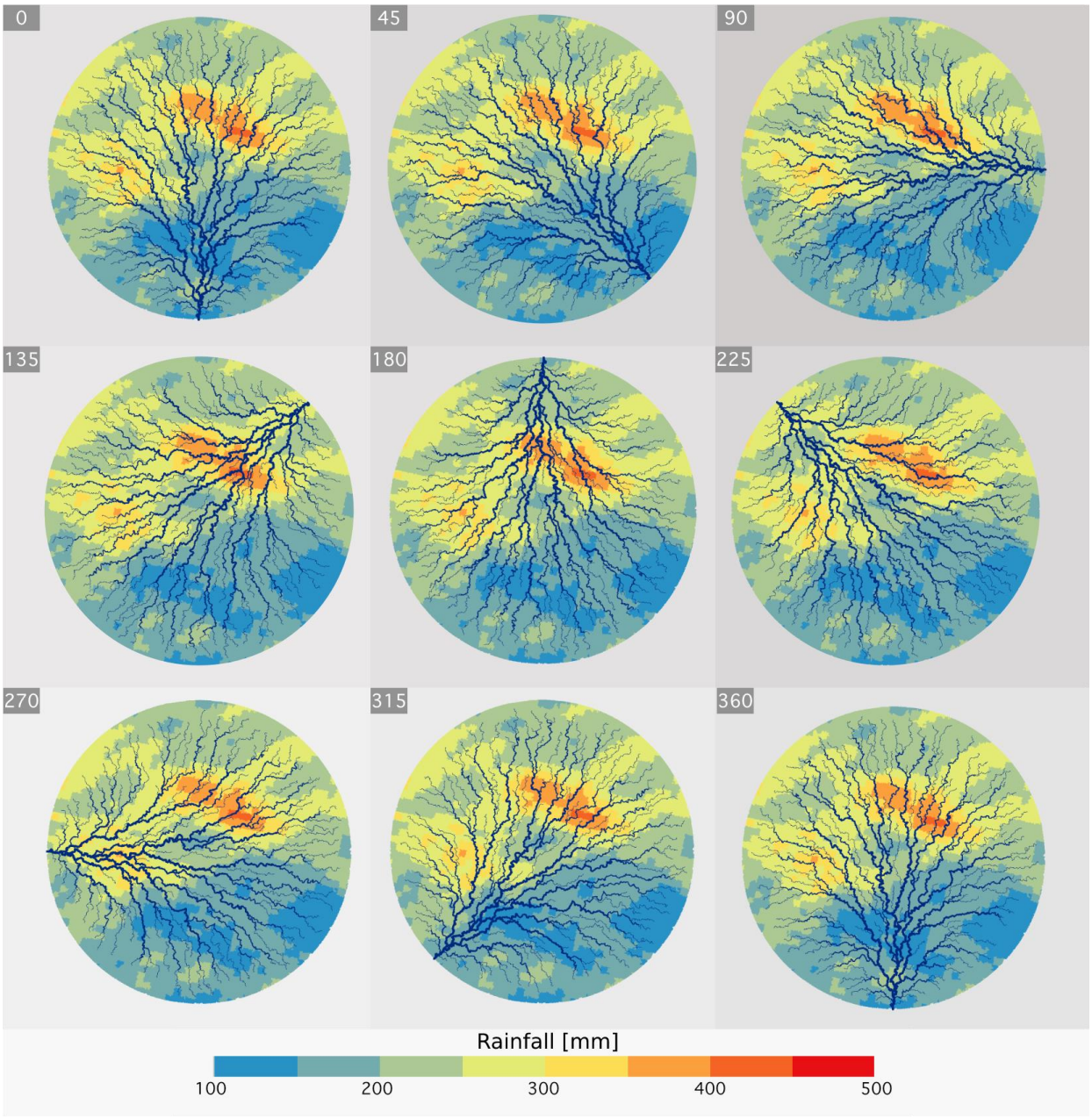

Figure 3: Demonstration of the interaction of rainfall with the river network. The rainfall shown here corresponds to the accumulation over September 2016. Each panel shows the interaction of rainfall with the river network of the circular basin upon rotation at every 45º in the counterclockwise direction, respectively.

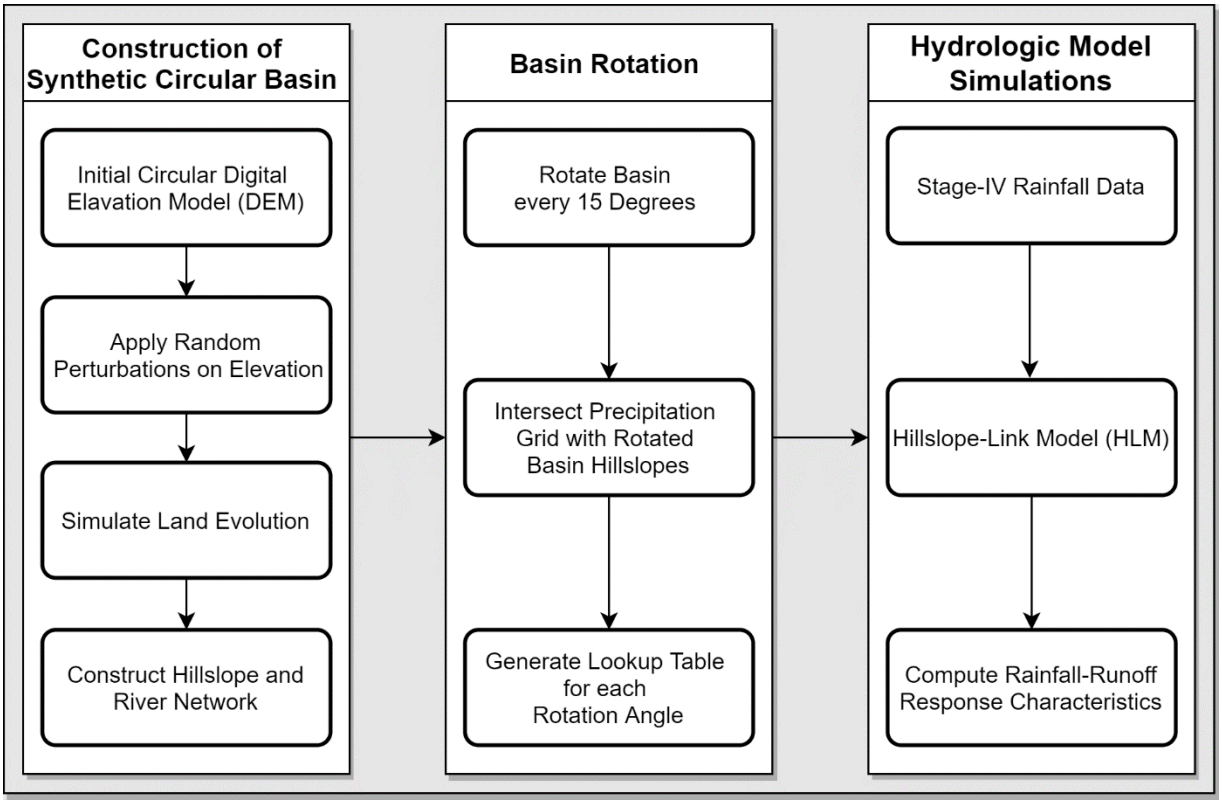

630

631 Figure 4: Flow chart depicting the methodology adopted in the study.

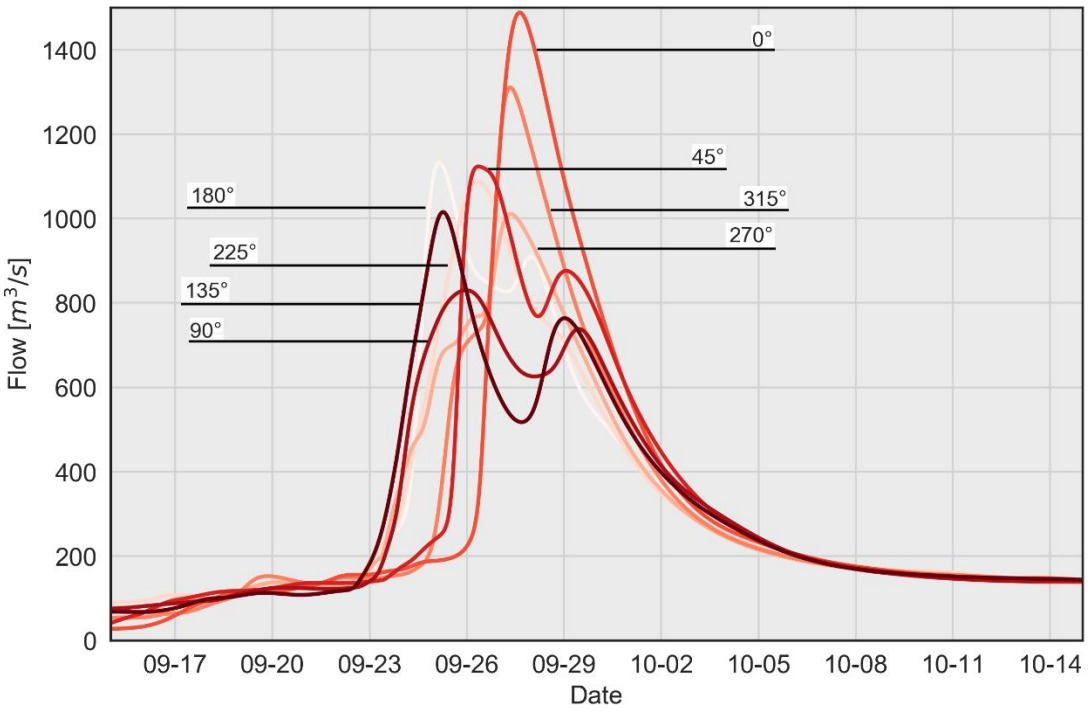

632

633 Figure 5: Illustration of simulation hydrographs at the basin outlet for the major event in

634 September 2016. The color code corresponds to the streamflow hydrograph for different angles

635 of basin rotation (refer to the labels in the figure).

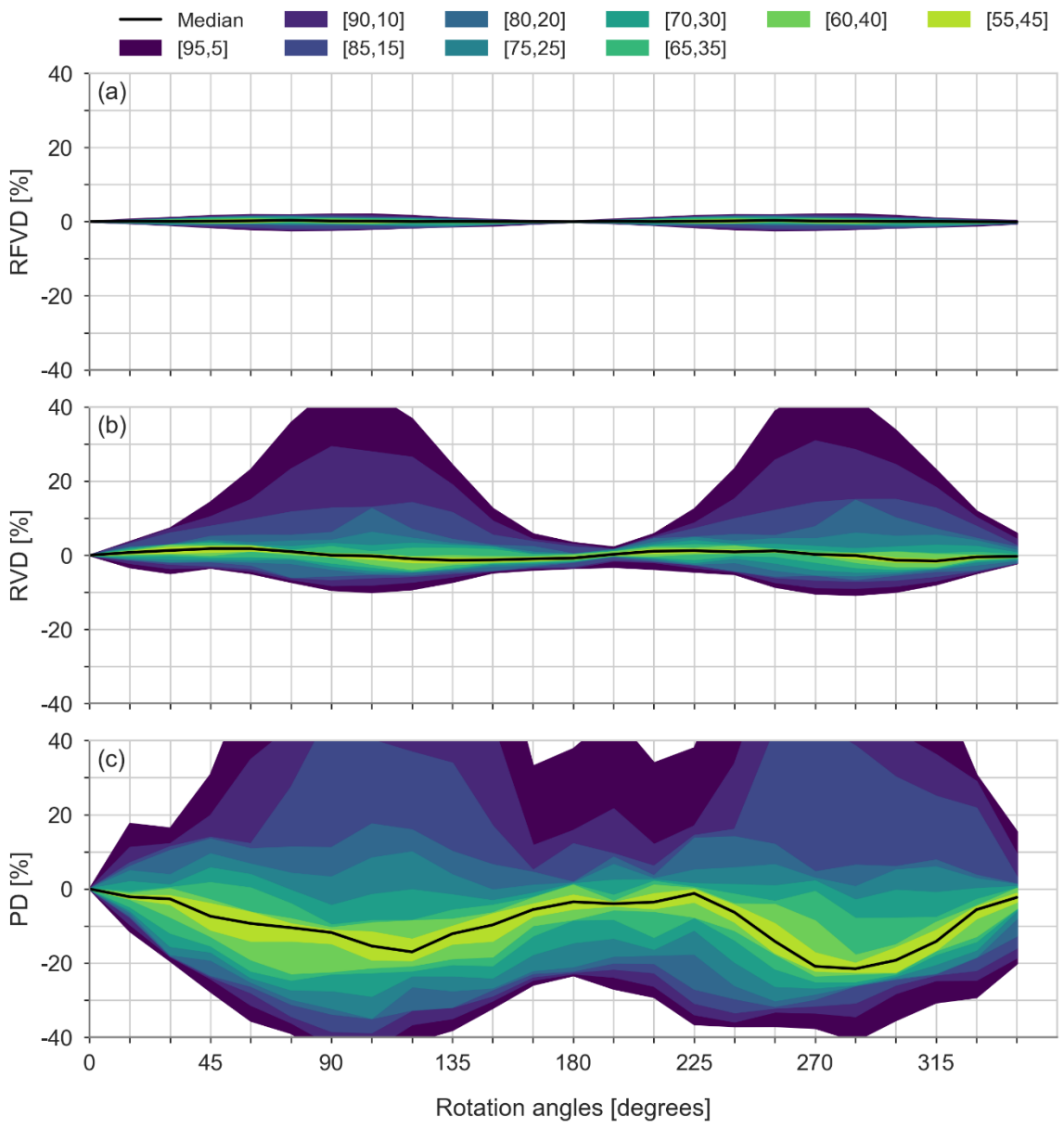

Figure 6: Percentile plots showing the relationship of rainfall-runoff metrics with angles of basin rotation evaluated at an annual scale. Each color code represents percentiles of interannual variability over the years 2003-2018 with every 5-percentile interval. For instance, [95,5] represents the range between 95th and 5th percentiles, [75,25] represents the range between 75th and 5th percentiles (i.e., interquartile range), and so on. (a) Rainfall volume difference (*RFVD*) (b) Runoff volume difference (*RVD*), and (c) Peak difference (*PD*).

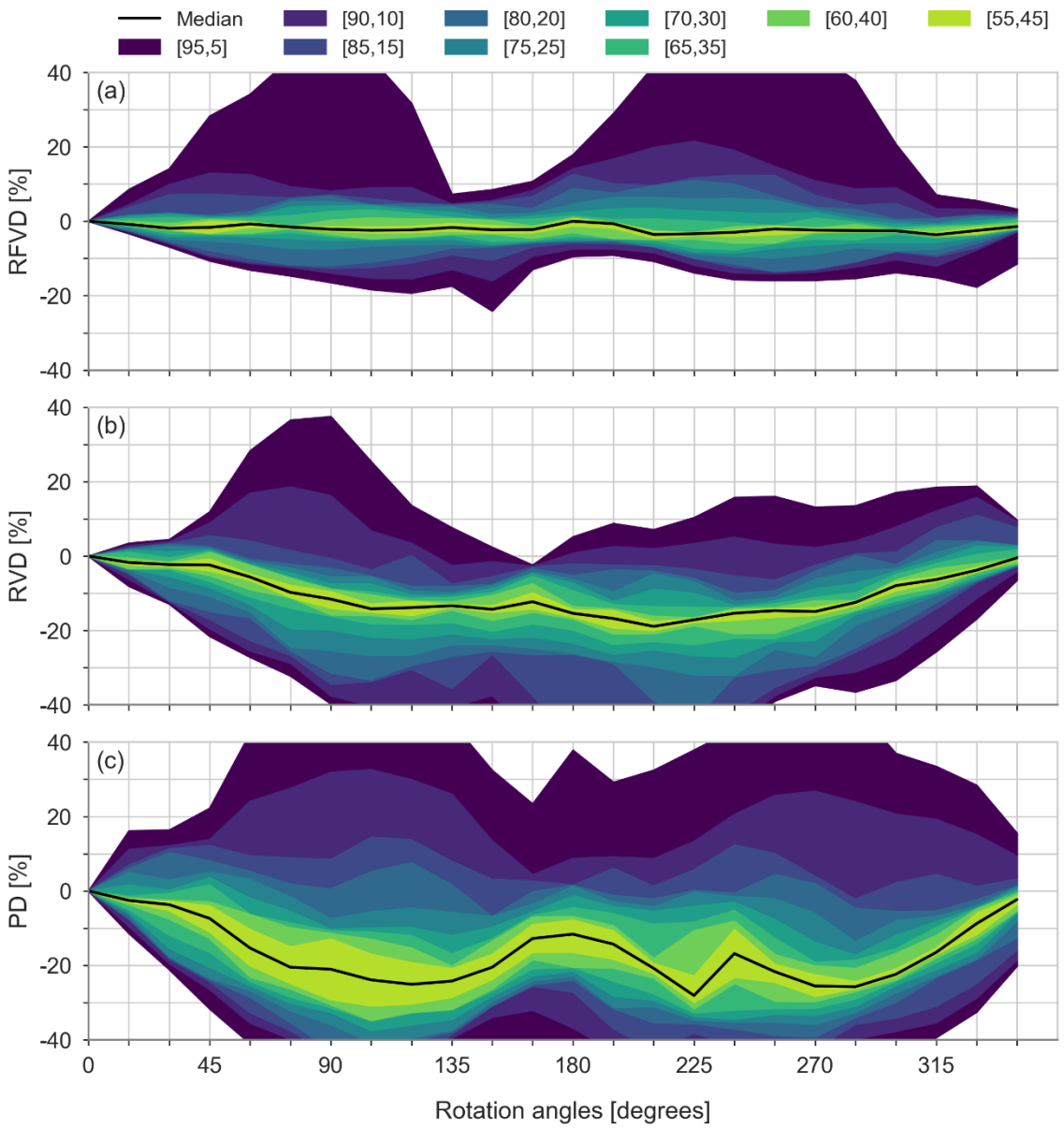

643

644 Figure 7: Percentile plots showing the relationship of rainfall-runoff metrics with angles of basin
645 rotation evaluated for the annual peak event. Each color code represents percentiles of
646 interannual variability over the years 2003-2018 with every 5-percentile interval. For instance,
647 [95,5] represents the range between 95th and 5th percentiles, [75,25] represents the range between
648 75th and 5th percentiles (i.e., interquartile range), and so on. (a) *RFVD* (b) *RVD*, and (c) *PD*.

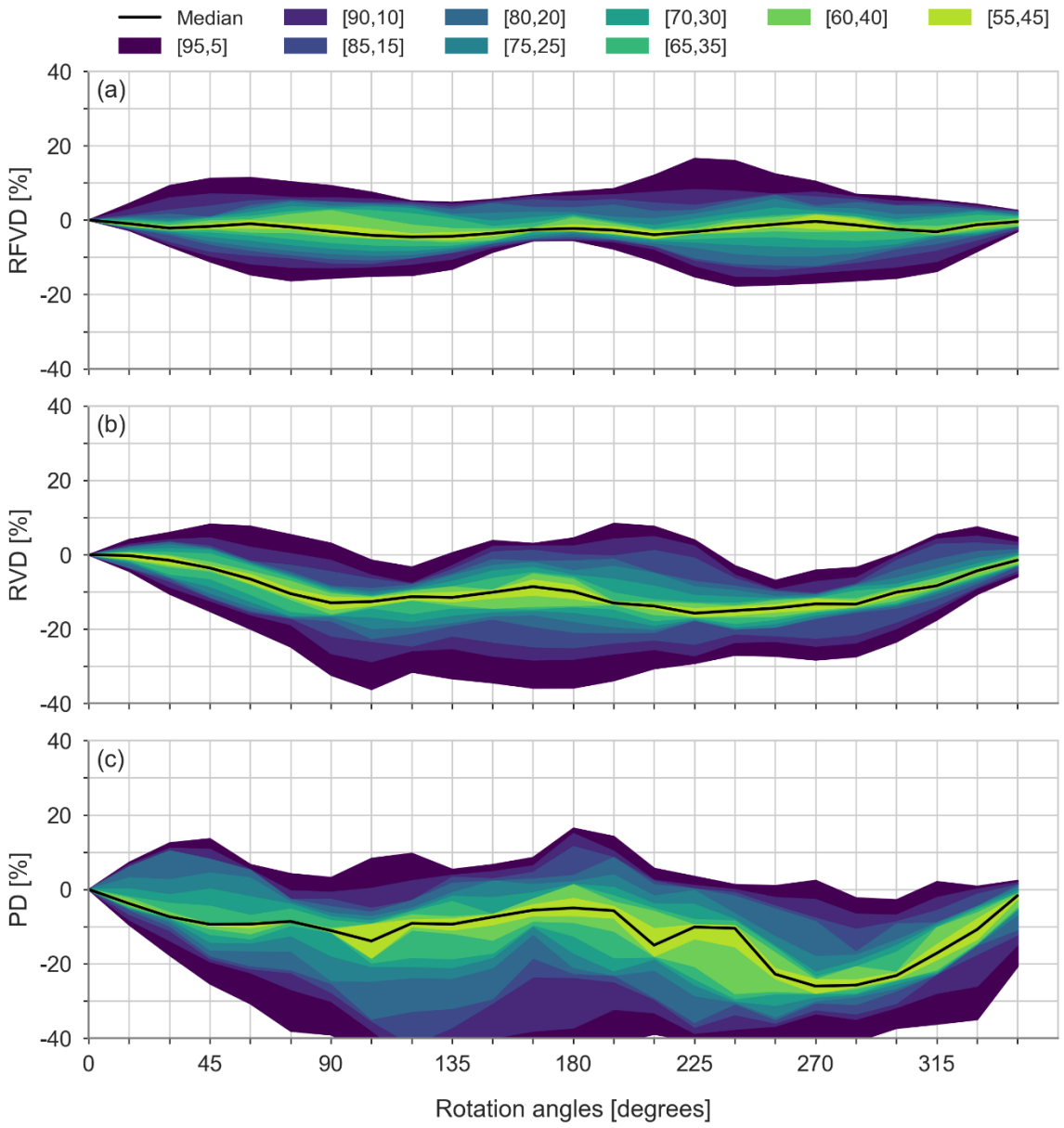

Figure 8: Percentile plots showing the relationship of rainfall-runoff metrics with angles of basin rotation evaluated for multiple peaks over the threshold. Each color code represents percentiles of interannual variability over the years 2003-2018 with every 5-percentile interval. For instance, [95,5] represents the range between 95th and 5th percentiles, [75,25] represents the range between 75th and 5th percentiles (i.e., interquartile range), and so on. (a) *RFVD* (b) *RVD*, and (c) *PD*.